A Deterministic Ray Tube Method for Microcellular Wave Propagation Prediction Model

Hae-Won Son and Noh-Hoon Myung

***Abstract*— In this paper, we present a new and very fast ray-tracing method using a ray tube tree, which is based on uniform geometrical theory of diffraction (UTD) and can solve some of the problems that other ray-tracing methods have. It is developed for quasi three-dimensional (3-D) environments and can be applied to any complex propagation environment composed of arbitrary-shaped buildings and streets. It finds all propagation paths from a transmitter to a receiver extensively with very high computation efficiency. It is fundamentally a point-to-point tracing method, so reception tests are not required and it guarantees high accuracy. To validate our ray-tracing method, signal path loss and root mean square (rms) delay spread were computed in the downtown core of Ottawa, Canada, and they were also compared with the published measurements. The results of the proposed method in this paper show good agreement with the measurements. The computation time required to obtain a path loss map in the site reveals very short in comparison with other methods.**

***Index Terms*— Cellular radio, electromagnetic wave propagation, geometrical theory of diffraction, ray tracing, urban areas.**

I. Introduction

As the demand for cellular radio services has increased dramatically in recent years, new cellular systems are needed to accommodate much more users with limited resource of frequency. This has resulted in the development of microcellular systems in which the cell size is much less than that of the current cellular systems and the base stations are placed at street-lamp level. The successful implementation of these systems requires the exact understanding of electromagnetic wave propagation mechanism such as path loss and delay spread characteristics. For this purpose, it is important to make propagation models which can predict propagation characteristics for various environments.

To characterize the microcell propagation, uniform geometrical theory of diffraction (UTD) and ray-tracing techniques are often employed as a theoretical prediction model because it provides much more accurate solution than other models together with its simplicity in analysis. It has been reported that the theoretical and empirical results were in very good agreement. Several propagation models based on the ray tracing techniques have been reported, which employ image concept and "brute force" ray tracing [1]–[14]. However, they present some limitations in the prediction modeling. In the brute force ray tracing, a large number of rays with a constant angular separation between neighboring rays are launched from a transmitter and intersection tests are performed for each ray on every scatter to determine the scattering points. After locating each scattering point, the reception test is performed, which is based on the reception sphere concept. This method is successfully applicable to complex environments, but the enormous computation time and memory are required due to a large number of rays and tests. Furthermore, the accuracy of the predicted result depends on the separation angle very sensitively. Image method, however, does not require the reception tests. It is a point-to-point tracing technique and provides accurate results. It also has very good computation efficiency because the rays which do not reach a receiver are not considered for the computation from the first. However, the selection of the scatters to generate the images is very difficult for complex environments, so it has been applied only to simple structures, for example, a city-street grid, etc. Recently, some approaches have tried to overcome this problem. In [13], the authors used "test rays" to find the scatters generating images, but their test rays are based on the brute force ray-tracing method, which provides no guarantee of including all possible propagation paths. In addition, the method also requires more excessive computation time than the previous image method. As another ray-tracing method, a "visibility tree" (VT) concept was reported [14]. The VT method can be used for any propagation environment because the path selection process does not depend on the particular geometery. Since all the propagation paths found from the VT do not give rise to real paths exactly, however, the method requires redundant computation time excessively to examine whether the selected path processes on VT are real or not by testing if the scattering points satisfying Fermat's principle are located on the corresponding scatters or not.

In this paper, we have developed a new ray-tracing method that can overcome the abovementioned limitations. Our method can be used for any complex propagation environment and find all propagation paths from a transmitter to a receiver extensively without redundant computations. In addition, since it is fundamentally a point-to-point tracing technique based on the image concept, it does not require reception tests and guarantees high accuracy. Its computation efficiency is also as high as the image method.

Manuscript received April 22, 1997; revised May 24, 1999.

The authors are with the Department of Electrical Engineering, Korea Advanced Institute of Science and Technology (KAIST), Yusong-gu, Taejon, Korea.

Publisher Item Identifier S 0018-926X(99)07967-3.

II. Theory and Formulation

The proposed method in this paper is developed for a quasi three-dimensional (3-D) environment, i.e., building walls

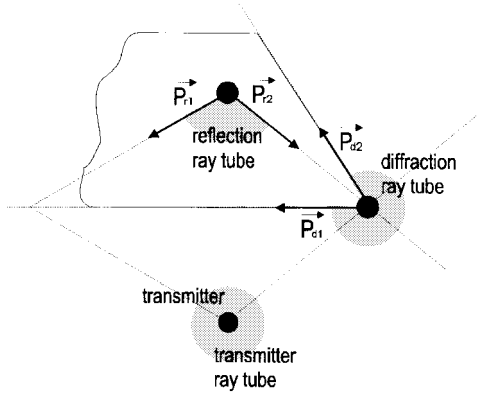

Fig. 1. Three types of ray tubes.

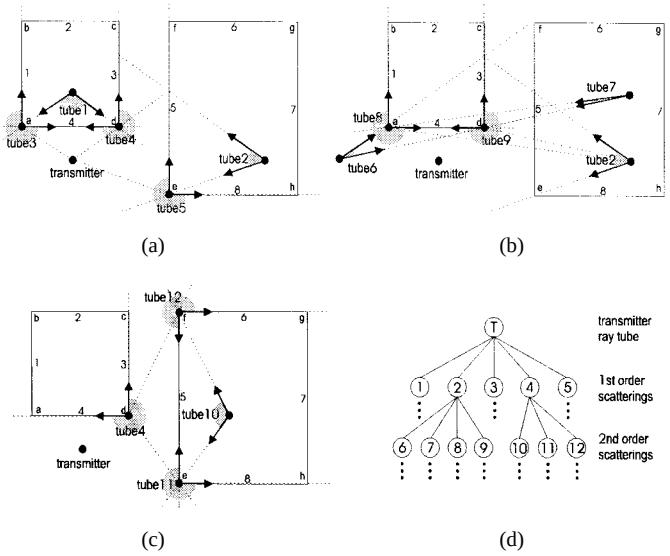

Fig. 2. An example of constructing a ray tube tree. (a) Children of the transmitter ray tube. (b) Children of the reflection ray tube 2. (c) Children of the diffraction ray tube 4. (d) Ray tube tree.

are assumed to be much higher than a transmitter height so that diffractions from the rooftops are neglected. All the propagation paths with possible combinations of wall and ground reflections and corner diffractions can be found by a systematic and unified process.

A. Three Types of Ray Tubes

To illustrate our method, three types of ray tubes must be defined; the transmitter, reflection, and diffraction ray tubes on the plane view of the quasi 3-D environment and they are generated from site-specific information.

The transmitter ray tube represents bundle of rays from a transmitter and is described by the position of the transmitter and the tube angle of 2π radian. It has an irregular shape because of the blockage of surrounding walls and corners. This blockage of the tube generates reflected and diffracted rays and the reflection and diffraction ray tubes are defined to represent these rays.

The reflection ray tube represents bundle of rays reflected by wall. It is described by the position of the image on the wall, the wall number and the tube angle less than π radian. Its image is one of the multiple reflected images of the transmitter or building corners as secondary sources. The tube angle is determined by the illuminated portion of the wall and represented by two unit vectors $\vec{P_{r_1}}$ and $\vec{P_{r_2}}$, as shown in Fig. 1. Basically, it has a fan-like shape but its valid region is confined by the corresponding wall and the blockage of walls and corners in its interior region. The reflection ray tube can be generated by all kinds of precedent ray tubes when they illuminate the wall in their interior region.

The diffraction ray tube is consisted of family of rays diffracted by corner and is generated as a child of three types of precedent ray tubes. It is described by the position of the corner, the corner number, and the tube angle. The position of the corner is used as its apex. The tube angle is determinded by two walls adjacent to the corner and described by two unit vectors $\vec{P_{d_1}}$ and $\vec{P_{d_2}}$, as shown in Fig. 1. It also has a fan-like shape, basically, but its valid region is confined by the blockage of other scatters in its interior region and its children tubes are generated from the blockage of these scatters.

For any complex propagation environment, the tree structure of the three types of ray tubes can be constructed always from its site-specific information. Unlike conventional image methods, predefined ray tubes have informations of their angular extents and valid regions as well as their apex positions, which corresponds to image positions in image methods, so their children ray tubes can be easily generated from site-specific information. In addition, our method treats reflected and diffracted rays as the same manner using ray tubes, so any combinations of reflections and diffractions can be found by a simple and unified process.

B. Construction of a Ray Tube Tree

The root of a ray tube tree is always the transmitter ray tube and it generates reflection and diffraction ray tubes as its children from surrounding walls and corners. Each of children also generates other reflection and diffraction ray tubes as its children. This recursive process continues until the depth of the tree is equivalent to $N+1$, where N is the order of scatterings composed of reflections and diffractions.

Fig. 2 shows an example of the constructing a ray tube tree for the plane view of a simplified environment made of two rectangular buildings. Each building has four walls and four corners. The walls are numbered from "1 to 8" and the corners are labeled with the alphabet from "a to h." The transmitter is located under the wall 4 and generates the transmitter ray tube, which is the root of the ray tube tree.

As the first order of scatterings, the transmitter ray tube is blocked by two walls: 4 and 5; and three corners: a, d, and e. Therefore, two reflection ray tubes from two blocking walls and three diffraction ray tubes from three blocking corners are generated as shown in Fig. 2(a). As the second order of scatterings, each of the previous five ray tubes generates reflection and diffraction ray tubes as its children. For example, the reflection ray tube 2 is blocked by two walls: 3 and 4; and two corners: a and d, so it generates two reflection and two diffraction ray tubes as shown in Fig. 2(b), whereas the diffraction ray tube 4 is blocked by one wall and two

corners and it generates accordingly one reflection ray tube and two diffraction ray tubes, as shown in Fig. 2(c). If the corners a and c are added to the blocking corners for the tube 4, double diffraction by two adjacent corners should be considered. By repeating this recursive process, it is possible to complete the ray tube tree with the depth corresponding to the order of scatterings. Fig. 2(d) shows an example of the ray tube tree constructed from the above process. The depth of the tree is 3, which accounts for the second-order of scatterings.

In the process of constructing the tree, various criteria are employed as well as the limitation of the scattering order. The generation of each branch can be limited by specifying the number of diffractions included in the Nth-order scatterings or discarding the ray tubes, which have field strength below a certain threshold value. The field strength of ray tubes can be calculated approximately on the plane view.

C. Finding Propagation Paths

Once the ray tube tree is completed, ray-tracing is employed to find all the propagation paths. Since the construction of the ray tube tree is independent of the location of a receiver, the tree can be used for any receiver location without reconstructing it.

The process of finding all the propagation paths is as follows. For a given location of a receiver, one may search the ray tubes enclosing the receiver by traversing the tree. For each tube enclosing the receiver, the sequence of the tubes from it to the transmitter ray tube can be founded in the tree. There may be a number of sequences and each of them gives one propagation path on the plane view. For each sequence of the tubes, reflection or diffraction points are calculated by backward ray tracing. Since the tube sequence provides the corresponding propagation path exactly, one doesn't have to check its physical reality unlike other methods. This advantage makes the computation efficiency of our method much higher.

To illustrate the versatility of our method, an example of ray tracing in a complex environment is shown in Fig. 3. It is the plane view of the KAIST, which has many arbitrarily shaped buildings. To find propagation paths, scatterings up to tenth order are considered together with the first order of diffraction.

D. Conversion of 2-D to 3-D Paths

After completion of the ray tube tree and derivation of all the propagation paths from it, the propagation paths on the plane view can be converted to 3-D ones. One propagation path on the plane view represents two 3-D paths, i.e., one is a free-space path and the other is a ground-reflected path. They are distinguished by the calculation of the heights of scattering points and it is performed using the total propagation path length on the plane view and two antenna heights. Fig. 4 shows an example of the conversion from one two-dimensional (2-D) path to two 3-D paths. The ground reflected path is calculated using the image of the transmitter as shown in the figure. In this process, the scattering points satisfying the laws of reflection and diffraction are found exactly for 3-D case.

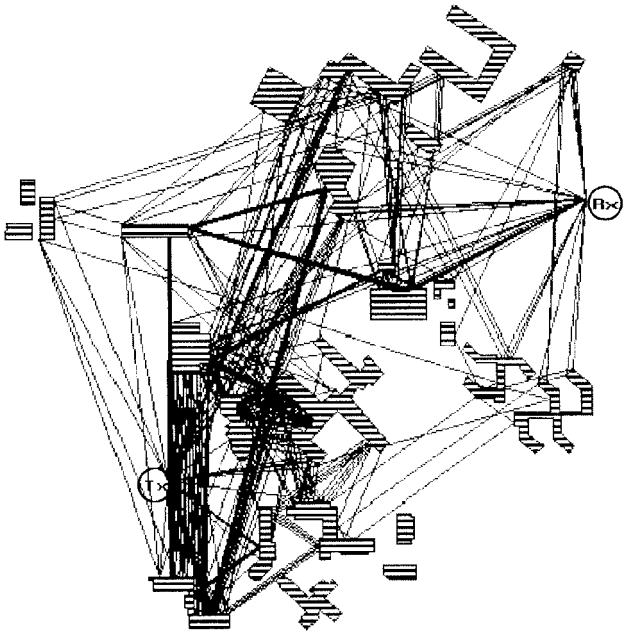

Fig. 3. An example of ray tracing in campus of KAIST.

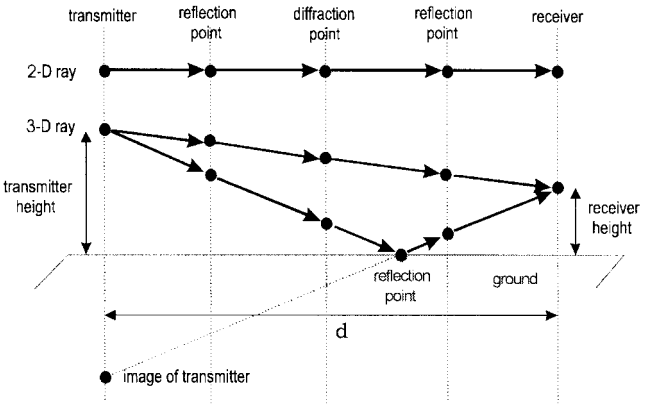

Fig. 4. Conversion of two-dimensional (2-D) to 3-D rays.

E. UTD Formulation

As a final step, one needs to derive the expressions for the fields contributed by each propagation path [18]–[20]. For a reflection or diffraction at a point Q, the incident field $E^i(Q)$ gives rise to a reflected field $E^r(P)$ or diffracted field $E^d(P)$ at a point P given by

$$E^r(P) = E^i(Q) R A_s e^{-jks} \tag{1}$$

$$E^d(P) = E^i(Q) D A_d e^{-jks} \tag{2}$$

where each parameter is meant by

- R dyadic reflection coefficient;
- D dyadic diffraction coefficient;
- A_s spreading factor for a reflection from a surface;
- A_d spreading factor for a diffraction at an edge;
- k propagation constant $= 2\pi/\lambda$;
- λ wavelength;
- s distance from Q to P.

Fig. 5. Plane view of the downtown core of Ottawa, Canada.

The expressions for R, D, A_s, and A_d are given in the Appendix. The contribution to the field E (at a receiver) due to a particular propagation path can then be obtained by successive application of the above equation. Contributions from all the propagation paths are determined and vectorially summed to give the total field at a receiver.

III. Results

A. Path Loss

To validate the proposed ray-tracing method in this paper, we have computed the signal path loss in Ottawa, Canada and compared it with the published measurements by Whitteker [15]. The measurements were made at 910 MHz with low antennas in the downtown core of the city, which is a typical urban area with arbitrarily shaped high buildings and open spaces. The transmitting and receiving antennas were vertical monopoles on small ground planes and placed at 8.5 and 3.65 m above ground, respectively. Signal strength was measured as a function of distance when the receiving van was driven along the streets within 900-m $\times$ 600-m rectangles. The map of the area in which the measurements were made is shown in Fig. 5. Street names and the outlines of buildings are shown and the heights of buildings may be judged roughly from the area they occupy. That is, buildings that fill a large fraction of the space between streets are many stories high and those occupying only a small area are typically three stories. All of them are higher than the transmitting antenna. The measurements were made for three different transmitter sites, but we chose only one site among them as shown in Fig. 5. Building walls and corners as well as the ground were modeled as nonperfect dielectric surfaces and edges. The values of relative permittivity ϵ_r and conductivity σ was chosen as 9, 0.1 S/m for buildings and 15, 7 S/m for the ground. The order of scatterings was limited to ten including the first order of diffraction. In addition, we discarded the ray tubes to give rise to path loss more than 150 dB by calculating the strength of ray tubes on a plane view. The antenna height, radiation pattern, and polarization were taken into account in the calculations.

Fig. 6 presents a path loss map of the area for a given transmitter location. To obtain the result, the tree composed of one transmitter ray tube, 252 868 reflection ray tubes, and 784 diffraction ray tubes was constructed. It took 297 s to construct the tree with the DEC Alpha Workstation. After constructing the tree, signal path loss was computed on 12 508 locations of receivers with the separation of 5 m between neighboring locations to make the path loss map shown in Fig. 6. The computation time required to complete the map was 934 s, i.e., 0.075 s per receiver location. It is extremely fast compared with the published result of 25 min per receiver location for 100 buildings, which employed image concept with test rays [13]. In our calculations, 130 buildings, with 614 walls and corners in total, were considered.

The detailed comparisons of our results and the measurements are shown in Figs. 7–9 and there are good agreements between them. Figs. 7 and 8 show the path loss along Slater and Laurier Streets. The former is a line-of-sight (LOS) street and the latter is an out-of-sight (OOS) street. On Laurier Street, it is seen that the path loss is highly dependent on the geometries and distributions of buildings. There are local peaks of signals where the open areas allow stronger signals to reach the street. In these comparisons, the predicted path loss is slightly less than the measurements. This is because we have no detailed information of the buildings and streets in this area and the effects of other scatters such as trees and vehicles are not taken into account in our calculations, either. On Slater Street, the truncation of the measured path loss within 20 m of the transmitter is due to receiver saturation. Fig. 9 shows the path loss along Queen Street which is an OOS street. On Queen Street, the errors between our results and measurements are a little larger than those on the other streets. This is because rooftop diffractions are ignored in the present analysis as mentioned earlier. Rooftop diffracted signals give large portion of total received signals when there are many obstructors between a transmitter and a receiver and so 2-D propagation paths have high attenuation. Table I shows the means and standard deviations of errors between our results and measurements on the three streets.

B. Delay Spread

One of the parameters to characterize wide-band multipath channels is their rms delay spreads. Delay spread can have determinantal effects on digital mobile radio systems, perticularly on relatively high bit-rate systems. The rms delay spread is the square root of the second central moment of power delay profile and calculated as in [16].

In this paper, rms delay spread has been analyzed as a function of path loss and compared with published measurements [17]. In [17], authors presented results of wide-band path loss and delay spread measurements for five representive microcellular environments in the San Francisco Bay area at 1900 MHz and developed a simple exponential overbound model for the worst-case estimation of delay spread as a function of path loss. Fig. 10 shows predicted rms delay spread as a function of path loss in the downtown core of Ottawa at 1900 MHz. Transmitting antenna heights of 3.7 and 8.5 m were tested with a receiving antenna height of 1.7 m. Receving antennas are uniformly distributed in this area and path loss up to 123 dB was considered. Other

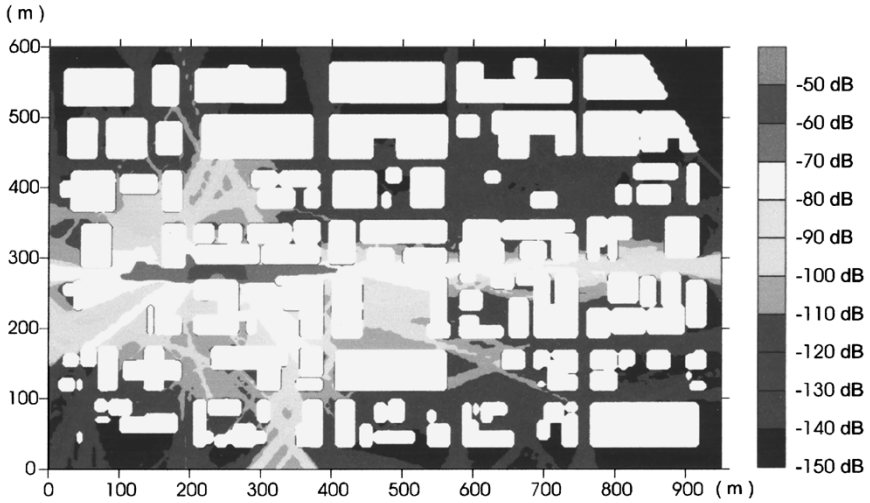

Fig. 6. Path loss map of Fig. 5.

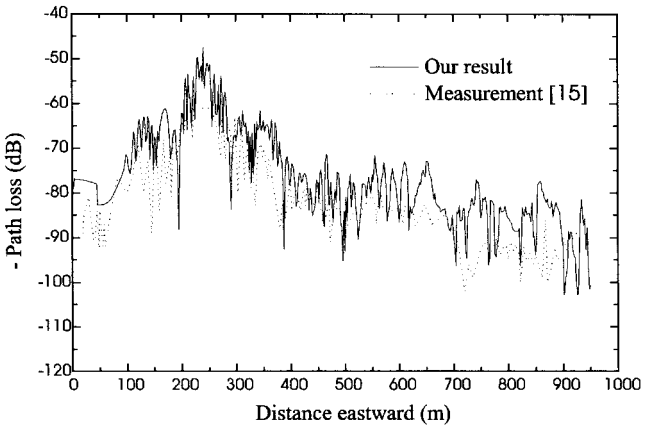

Fig. 7. Path loss in Slater Street.

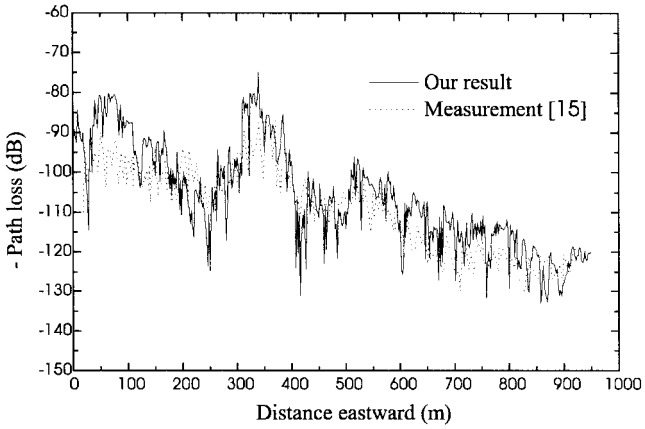

Fig. 8. Path loss in Laurier Street.

parameters needed in our model are the same with those used in the previous path loss calculations. From the figure, it is clear that our predicted results satisfy the proposed exponential overbound model of the form $\sigma_d = e^{0.065\mathrm{PL}}$, where σ_d is the rms delay spread in nanoseconds and PL is the path loss in decibels. Table II shows the mean and standard deviations of the rms delay spread for the two transmitting

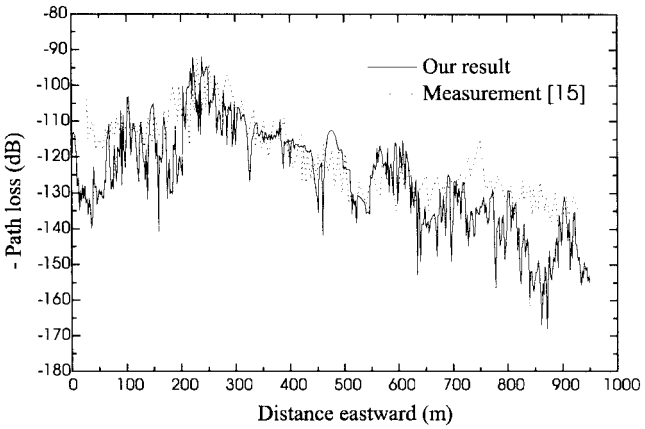

Fig. 9. Path loss in Queen Street.

TABLE I
MEANS AND STANDARD DEVIATIONS OF ERRORS BETWEEN PREDICTIONS AND MEASUREMENTS ON THE THREE STREETS

Street	Slater St.	Laurier St.	Queen St.
Mean	6.13 dB	3.22 dB	-4.86 dB
Standard Deviation	6.14 dB	7.42 dB	10.50 dB

antenna heights. The low antenna at 3.7 m have an average rms delay spread of 134.6 ns, whereas the high antenna at 8.5 m have an average rms delay spread of 173.1 ns. The delay spread increases as the antenna height increases because as the antenna height increases, propagation channel characteristics are affected by more scattering objects at greater distances. Table II also shows measured rms delay spread values in typical microcellular environments [17] and there are good agreements between the measurements and our predicted results in Ottawa.

IV. CONCLUSION

In this paper, we present a new ray-tracing method using ray tubes. Our method can be applied to any complex

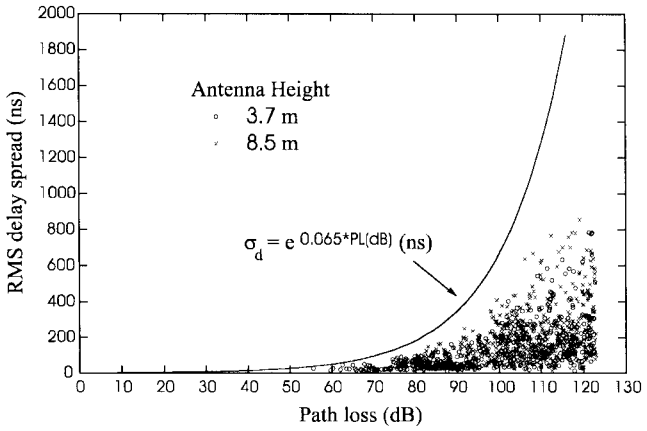

Fig. 10. Path loss versus rms delay spread.

TABLE II
MEANS AND STANDARD DEVIATIONS OF THE RMS DELAY SPREADS OF OUR RESULTS IN OTTAWA AND MEASUREMENTS IN SAN FRANCISCO

Antenna height	Our results (Ottawa)		Measurements [17] (San Francisco)	
	Mean RMS delay spread	Standard deviation	Mean RMS delay spread	Standard deviation
3.7 m	134.6 ns	127.4 ns	136.8 ns	138.0 ns
8.5 m	173.1 ns	156.8 ns	176.8 ns	147.1 ns

propagation environment and find all the propagation paths from a transmitter to a receiver exhaustively without redundant computations, i.e., reception tests or existence tests of paths, which can provide enormous computation efficiency. Furthermore, it guarantees high accuracy because it is fundamentally a point-to-point tracing technique. The proposed method in this paper is developed based on quasi 3-D environments. However, it can be applied to 3-D environments completely if one extends the ray tubes to 3-D ones. In addition, by properly manipulating the process of constructing the ray tube tree, our method can also include transmission ray tubes in the tree, which can then be applied to indoor environments.

APPENDIX

The expressions for the terms in (1) and (2) are listed below [20]:

$$R = R_s e^i_\perp e^r_\perp + R_h e^i_\parallel e^r_\parallel$$

$$R_s(\theta,\epsilon') = \frac{\cos\theta - \sqrt{\epsilon' - \sin^2\theta}}{\cos\theta + \sqrt{\epsilon' - \sin^2\theta}}$$

$$R_h(\theta,\epsilon') = \frac{\epsilon'\cos\theta - \sqrt{\epsilon' - \sin^2\theta}}{\epsilon'\cos\theta + \sqrt{\epsilon' - \sin^2\theta}}$$

$$\epsilon' = \epsilon_r - j\frac{\sigma}{\omega\epsilon_0}$$

$$D = -D_s\beta_0^2 - D_h\phi'\phi$$

$$D_{s,h} = D_1 + D_2 + R_{s,h}(D_3 + D_4)$$

$$D_1(L,\phi,\phi',\beta_0,n) = -\frac{e^{-j(\pi/4)}}{2n\sqrt{2\pi k}\sin\beta_0}\cot\left[\frac{\pi+(\phi-\phi')}{2n}\right] \times F[kLa^+(\phi-\phi')]$$

$$D_2(L,\phi,\phi',\beta_0,n) = -\frac{e^{-j(\pi/4)}}{2n\sqrt{2\pi k}\sin\beta_0}\cot\left[\frac{\pi-(\phi-\phi')}{2n}\right] \times F[kLa^-(\phi-\phi')]$$

$$D_3(L,\phi,\phi',\beta_0,n) = -\frac{e^{-j(\pi/4)}}{2n\sqrt{2\pi k}\sin\beta_0}\cot\left[\frac{\pi+(\phi+\phi')}{2n}\right] \times F[kLa^+(\phi+\phi')]$$

$$D_4(L,\phi,\phi',\beta_0,n) = -\frac{e^{-j(\pi/4)}}{2n\sqrt{2\pi k}\sin\beta_0}\cot\left[\frac{\pi-(\phi+\phi')}{2n}\right] \times F[kLa^-(\phi+\phi')]$$

$$F(x) = 2j\sqrt{x}\int_{\sqrt{x}}^{\infty} e^{-ju^2}\,du \quad \text{for } x > 0$$

$$F(x) = F^*(|x|) \quad \text{for } x < 0$$

$$a^\pm(\phi,\phi') = 2\cos^2\left[\frac{2\pi nN^\pm - (\phi\pm\phi')}{2}\right]$$

$N^\pm$ = integer that most nearly satisfy the following two equations

$$2\pi nN^+ - (\phi\pm\phi') = \pi$$

$$2\pi nN^- - (\phi\pm\phi') = -\pi$$

$$n = \frac{2\pi-\alpha}{\pi}$$

α = interior wedge angle

$$A_s(s) = \frac{\rho}{s+\rho}$$

$$A_d(s) = \sqrt{\frac{\rho}{s(\rho+s)}}.$$

REFERENCES

[1] V. Erceg, S. Ghassemzadeh, M. Taylor, D. Li, and D. L. Schilling, "Urban/suburban out-of-sight propagation modeling," *IEEE Communicat. Mag.*, vol. 30, pp. 56–61, June 1992.

[2] V. Erceg, A. J. Rustako, and R. S. Roman, "Diffraction around corners and its effects on the microcell coverage area in urban and suburban environments at 900 MHz, 2 GHz, and 6 GHz," *IEEE Trans. Veh. Technol.*, vol. 43, pp. 762–766, Aug. 1994.

[3] A. J. Rustako Jr., N. Amitay, G. J. Owens, and R. S. Roman, "Radio propagation at microwave frequencies for line-of-sight microcellular mobile and personal communications," *IEEE Trans. Veh. Technol.*, vol. 40, pp. 203–210, Feb. 1991.

[4] K. R. Schaubach, N. J. Davis, and T. S. Rappaport, "A ray tracing method for predicting path loss and delay spread in microcellular environments," in *42nd IEEE Veh. Technol. Conf.*, Denver, CO, May 1992, vol. 2, pp. 932–935.

[5] K. R. Schaubach and N. J. Davis, "Microcellular radio-channel propagation prediction," *IEEE Antennas Propagat. Mag.*, vol. 36, pp. 25–33, Aug. 1994.

[6] M. C. Lawton and J. P. McGeehan, "The application of GTD and ray launching techniques to channel modeling for cordless radio systems," in *42nd IEEE Veh. Technol. Conf.*, Denver, CO, May 1992, vol. 2, pp. 125–130.

[7] ——, "The application of a deterministic ray launching algorithm for the prediction of radio channel characteristics in small-cell environments," *IEEE Trans. Veh. Technol.*, vol. 43, pp. 955–969, Nov. 1994.

[8] C. Bergljung and L. G. Olsson, "Rigorous diffraction theory applied to street microcell propagation," in *IEEE Global Telecommunicat. Conf., GLOBECOM'91*, Phoenix, AZ, Dec. 1991, pp. 1292–1296.

[9] S. Y. Seidel and T. S. Pappaport, "Site-specific propagation prediction for wireless in-building personal communication system design," *IEEE Trans. Veh. Technol.*, vol. 43, pp. 879–891, Nov. 1994.

[10] S. Y. Tan and H. S. Tan, "UTD propagation model in an urban street scene for microcellular communications," *IEEE Trans. Electromagn. Compat.*, vol. 35, pp. 423–428, Nov. 1993.
[11] ——, "A theory for propagation path loss characteristics in a city street-grid," *IEEE Trans. Electromagn. Compat.*, vol. 37, pp. 333–342, Aug. 1993.
[12] ——, "Improved three-dimensional ray tracing technique for microcellular propagation models," *Electron. Lett.*, vol. 31, pp. 1503–1505, Aug. 1995.
[13] ——, "A microcellular communications propagation model based on the uniform theory of diffraction and multiple image theory," *IEEE Trans. Antennas Propagat.*, vol. 44, pp. 1317–1326, Oct. 1996.
[14] M. G. Sanchez, L. de Haro, A. G. Pino, and M. Calvo, "Exhaustive ray tracing algorithm for microcellular propagation prediction models," *Electron. Lett.*, vol. 32, pp. 624–625, Mar. 1996.
[15] J. H. Whitteker, "Measurements of path loss at 910 MHz for proposed microcell urban mobile systems," *IEEE Trans. Veh. Technol.*, vol. 37, pp. 125–129, Aug. 1988.
[16] D. C. Cox, "Delay Doppler characteristics of multipath propagation at 910 MHz in a suburban mobile radio environment," *IEEE Trans. Antennas Propagat.*, vol. AP-20, pp. 625–635, Sept. 1972.
[17] M. J. Feuerstein, K. L. Blackard, T. S. Rappaport, S. Y. Seidel, and H. H. Xia, "Path loss, delay spread, and outage models as functions of antenna height for microcellular system design," *IEEE Trans. Veh. Technol.*, vol. 43, pp. 487–498, Aug. 1994.
[18] R. J. Luebbers, "Finite conductivity uniform GTD versus knife edge diffraction in prediction of propagation path loss," *IEEE Trans. Antennas Propagat.*, vol. AP-32, pp. 70–76, Jan. 1984.
[19] P. D. Holm, "UTD-diffraction coefficients for higher order wedge diffracted fields," *IEEE Trans. Antennas Propagat.*, vol. 44, pp. 879–888, June 1996.
[20] D. A. McNamara, C. W. I. Pistorius, and J. A. G. Malherbe, *Introduction to the Uniform Geometrical Theory of Diffraction*. Boston, MA: Artech House, 1990.

Hae-Won Son was born in Taegu, Korea, in 1971. He received the B.S. degree in electronics engineering from the Kyungpook National University, Taegu, Korea, in 1994, and the M.S. degree in electrical engineering from the Korea Advanced Institute of Science and Technolgy (KAIST), Taejon, Korea, in 1996. He is currently working toward the Ph.D. degree in electrical engineering at the KAIST.

His current research interests include computational electromagnetics and theoretical prediction of wave propagation characteristics for mobile radio communications and broadcastings.

Noh-Hoon Myung was born in Seoul, Korea, in 1953. He received the B.S. degree in electrical engineering from the Seoul National University, Korea, in 1976, and the M.S. and Ph.D. degrees from the Ohio State University, Columbus, in 1982 and 1986, respectively.

He was a Research Member at the ElectroScience Laboratory, Ohio State University, for six years, working in the area of electromagnetic wave scattering and propagation before joining the Electrical Engineering Department, Korea Advanced Institute of Science and Technology (KAIST), as an Assistant Professor. He was also a member of the research staff of the National Highway Traffic and Safety Administration (NHTSA), Ohio, where he constructed a ground-based optical vehicle tracking system. His current research areas include wave scattering and propagation analysis, radar cross-section analysis, antenna and radar system design, mobile and satellite communications, and electromagnetic interference and electromagnetic compatibility (EMI/EMC).